JOINT EUROPEAN TORUS

JET–P(85)05

P.G. Carolan, M.J. Forrest, N.J. Peacock
and D.L. Trotman

Observation of Zeeman Splitting of Spectral Lines from the JET Plasma

Observation of Zeeman Splitting of Spectral Lines from the JET Plasma

P.G. Carolan, M.J. Forrest, N.J. Peacock
and D.L. Trotman

JET-Joint Undertaking, Culham Science Centre, OX14 3DB, Abingdon, UK

[1]*EURATOM/UKAEA Fusion Association, Culham Laboratory, OX14 3DB, Abingdon, OXON, UK*

Preprint of Paper to be submitted for publication in
Plasma Physics and Controlled Fusion

ABSTRACT.

Zeeman splitting of spectral lines from hydrogen and impurities in the JET tokamak plasma has been observed in the visible region of the spectrum. An Optical 'Multi channel Analyser (OMA) coupled to a 1m Czerny-Turner instrument is used to record several spectral lines simultaneously many times during a discharge. Tangential viewing optics enhance the influence of Zeeman splitting, especially when the impurities are located where the magnetic field is aligned along the viewing chord. To date, splitting of H_α (6563Å), CII (6578Å and 6583Å), Cri (4289Å, 4274Å and 4254Å) and Cl II (4794Å, 4810Å and 4819Å) has been detected. The location of the impurities is determined from the magnitude of the splitting and the known toroidal field distribution. The effects of the magnetic field on the line profiles are best observed during the plasma initiation and termination phases where, for example, a large plasma incursion can result in the injection of impurities from the inner wall. The technique is of particular importance in determining the source of impurities (e.g. from the inside wall or the limiter at the outer periphery). The observations also highlight the importance of taking Zeeman splitting into account when making Doppler shift or broadening measurements in the visible spectrum.

1. INTRODUCTION

There have been various suggestions for measuring the magnetic field strength, from the Zeeman splitting of spectral lines (e.g. Jahoda et al (1963) and Hubner (1964)) which involve seeding a plasma with impurities, or injecting them in as a beam (McCormick et al (1977)). However, it has often not been fully appreciated that the Zeeman splitting can also be important in interpreting line shifts and broadening of spectral lines from the atomic species which are normally present in a torus. This is especially the case when operating in the visible region of the emitted spectrum from tokamak plasmas.

The magnitude of Zeeman splitting is proportional to λ^2 while competing effects, such as Doppler shifts and Stark broadening, have a linear dependence on λ. Interpretation of line profile analysis should take account of not only the Zeeman effect but also the fine structure splitting, the translational Stark effect (Breton et al (1980)) and the detailed 'ℓ' shell population of the levels involved in the transitions (Fonck et al (1984)).

Profile analysis of the emission lines from hydrogen, in magnetic confinement machines, is a special and important case (e.g. charge exchange collisions between the ions and background neutrals enable ion temperature measurements to be made from the Balmer lines spectral wings). It has been treated in some detail by Breton et al (1980) for high energy neutrals where the translational Stark effect, arising from the electric field generated in the neutral frame of reference, when it traverses the background magnetic field, is comparable to the Zeeman effect. Doppler effects are also included in the treatment. In the present study, only the low energy peripheral neutrals and ions are considered where the Zeeman effect dominates and Doppler effects are ignored.

The advantages of seeding a plasma with selected impurities, and preferably in a beam, are clear when very accurate field measurements are required (e.g. to measure both $B_{toroidal}$ and $B_{poloidal}$) but the Zeeman effect can also be turned to good effect in locating impurities

from the magnitude of the splitting when the spatial distribution of the magnetic field is known. The magnitude of the Zeeman splitting depends on the Lande 'g' factor of the term states involved in the transition, where the separation of the σ lines from the central π lines ranges from 1-2 x 4.67 x 10^{-9} $B\lambda^2$ (Å, tesla). By way of example, the transition with the largest Zeeman splitting factor observed to date from the JET tokamak (Rebut et al (1984)), the CII line at 6582.85Å ($^2S_{\frac{1}{2}} - {}^2P_{\frac{1}{2}}$), yields line shifts of 0.5Å at a field of 2T. This is substantially larger than that expected of Doppler shifts for this ion (the equivalent CII ion energy required is about 40ev). Thus, an instrument of only moderate resolution (FWHM $\simeq$ 0.5 - 1Å), as might be used in spectral survey applications, should detect the influence, at least, of Zeeman splitting on this line. (The neighbouring $H\alpha$ line at 6563Å has σ components which are separated by 0.4Å at 2T from the unshifted π components. The neutral energy required to give the same Doppler shift is 3ev whereas the fine structure splitting is 0.13Å).

In addition to the influence the magnetic field exerts on the line shape in terms of splitting, it is also important to consider the relative intensities of the π and σ Zeeman components, and how these vary with the viewing and magnetic field directions. The emitted light is polarised according to the inclination angle between magnetic field and viewing direction and the magnetic quantum numbers m, involved in the detailed transitions (i.e. π components entail transitions with $\Delta m = 0$ and σ components with $\Delta m = \pm 1$; the π components are plane polarised along the field directions and the σ components are, in general, elliptically polarised but are plane polarised perpendicular to the field when viewed at 90° to the field). Various means can be adopted to enhance or diminish the influence of Zeeman effects by, for example, the use of appropriate polarising and wavelength filters, or by varying the viewing direction with respect to the magnetic field. If the source of the line emissions can be restricted to localised volumes in the plasma, this will limit the smearing effects resulting from a distribution of field vectors, as seen along a viewing chord. For low ionisation states such a localisation can be found in plasma confinement machines when either the outer wall region (or limiter) or the inner plasma boundary dominates the emission. It was by having a bright thin volume of

suitable spectral lines and an appropriate viewing direction that Zeeman splitting effects were observed in the JET plasma and less so in the DITE plasma (Axon et al (1983)).

2. APPARATUS

The spectral instrument is shown in Fig.1. It consists of a 1 metre Czerny-Turner arrangement [Rank Hilger MONOSPEK - 1000], with a 1200 grooves/mm grating, which is coupled to an Optical Multichannel Analyser (OMA) (PARC) detector. High quality camera lenses [Telephoto lens (135 mm, f2.8) and a Zoom lens (70-150 mm, f3.8)] are used in a front-to-front configuration, with the OMA and the spectral plane of the spectrometer at the focal planes of the lenses. The light is relayed from a selection of JET viewing optics (cf. Fig.2 for a tangential viewing system) via 100 m of a single fibre optic link of 1mm diameter quartz. Similar arrangements with the same fibre type, were used with this instrument in the DITE tokamak and HBTX1A Reversed Field Pinch (Carolan et al (1984)) experiments.

The Zoom lens facility allowed for adjustments of the overall system in terms of spectral coverage, resolution and vignetting. It was found that all three were met satisfactorily with the f=70 mm (Zoom lens) and f=135 mm (Telephoto) combination. This arrangement gave a spectral coverage of about 75Å and had an optimum resolution performance of 0.3Å FWHM. The typical instrumental functions used for the three experiments DITE, JET and HBTXIA are shown in Fig.3. The 0.3Å FWHM and 0.7Å FWHM resolutions correspond to input slit widths of approximately 25 μm and 100 μm respectively. (There are slight differences in the overall dispersions, or wavelength interval per channel, between the machines because of detailed focusing of the lenses.)

The use of fibre optics ensures that unpolarised light is offered to the dispersive system. Any polarisation sensitivity of the instruments can thus be safely neglected (e.g. the reflectance of a grating differs depending on the direction of the plane of polarisation). Although the 'handedness' of circular polarisation will be retained when transmitted through the fibre optics, this has the

convenient attribute of maintaining equal weighting to its two orthogonally plane polarised components. The Optical Multichannel Analyser system consists of an OMA-2 by Princeton Applied Research and controlled by a Culham Laboratory Stand Alone Data Acquisition (SADA) system (C G Cross et al (1978)) . The detector photo cathode has a red enhanced response and has an active area of 2.5 mm x 18 mm with 25 μm wide channels. A 14 bit A.D.C. (1200 electrons ≈ 1 count ≈ 1 photo electron) digitizes the output of the cooled 1024 channel silicon photodiode array with a read rate of 16 μs/channel. The central 720 channels of the diode array are intensified by a micro channel plate. The SADA system consists of D.E.C. LSI11/23 processor, 32k word memory and two disc drives. The OMA is controlled via a Hytek 200 output register. Local data storage for spectral data is provided by a Le Croy MM 8206A with 64k (16 bit word) memory. The processor is also used to analyse the data and present them in a graphical form.

3. RESULTS

It was customary to have the OMA triggered at least one scan time before plasma initiation. The first scan could then be used to subtract the ambient background light from the subsequent scans. The shortest integration time used was 16.4 ms with intermediate ones at 50 ms. and 100 ms. For long JET shots ($\gtrsim$5 secs), 200 ms/scan was used. However, it was found that integration periods in excess of 50 msec tended to mask transient effects, in particular the Zeeman splitting of the spectral lines described below. The number of scans that were taken depended on the plasma duration and ranged from 3 scans for the HBTX1A experiment to 64 scans for JET.

The OMA spectrometer system was used on three different experiments, two of which were tokamaks (DITE and JET) and the other a Reversed Field Pinch device (HBTX1A). The total magnetic field differs by an order of magnitude between these two types of confinement systems with typically 2-3T in the former and 0.3T in the latter (cf. Section 5 below). In Fig.4 we show the same spectral region, at a CII doublet ($2s^2 3s\ ^2S_{1/2} - 3p^2P^0_{1/2,3/2}$), from the three machines. (The presence of carbon principally arises from the carbon limiters that are used to isolate the plasma from the metal wall). Because of the small

ionisation potential required in ionising to CIII (11eV), the radiation from CII primarily comes from the plasma edge. The outer edge magnetic fields were: HBTX1A:- 0.17T, DITE:-2.3T JET:-1.7T. Even from inspection, it can be seen that the spectral widths of the CII lines from the tokamak plasmas exceed those from the RFP plasma. It may also be noted, in the tokamak cases, that the CII line at 6583Å is noticably broader then the other CII line. (A extensive study of the behaviour of the CII lines, throughout the plasma duration and from many plasma shots excluded the possibility of the presence of significant spectral line blending.) Such a phenomenon cannot be explained by Doppler effects alone, which would require both of the CII lines to be similarly affected.

The clearest evidence of the splitting of spectral lines was seen in the JET experiment when the viewing chord was in the equatorial plane and parallel to a major circumference at its midpoint (as shown in Fig.2). This 'tangential' chord presents a clear view of the carbon limiter on the opposing side of the vacuum vessel and it can be noted that its midpoint is also relatively close to, but clear of, the inner wall.

Two sequences of OMA spectral scans taken at 50 ms intervals are shown in Figs. 5 and 6. The first scan shown in each set, is obtained from a typical period of a JET shot. The other scans were obtained during the termination phase of two discharges from the JET machine. In Fig.5 the CII doublet lines are seen to progressively broaden and split. The peak separation of the CII 6578Å line is about 20% less than that of the CII 6583Å line which is the line that normally has the broader line profile. The behaviour of the Hα line is similar to the CII but delayed in time and the depth of modulation is not as large. In Fig.6 splitting of the CrI multiplet ($3d^5 4s^7S_3 - 4p^7P^o_{2,3,4}$) lines is clearly seen. (The lack of splitting in the CrI line at 4254Å as we will show below, is simply a consequence of the convolving effect of the instrumental function and the smaller Zeeman splitting expected for this line). This multiplet provides the clearest evidence that the splitting cannot be explained by Doppler shifts since this would be the same for all the three lines. The CII line at 4267Å shows no such splitting and is discussed below.

In more recent discharges in the JET tokamak, splitting of CIII lines ($^5S_2$ - $^5P_{1,2,3}$; 4819.46Å, 4810.06Å, 4794.54Å) has been observed in the termination phase of a long (~9 secs) discharge. The spectra can be seen in Fig.7. The uppermost spectrum (Scan 48) is typical for that particular shot. In the bottom two spectra the line intensity increases but, in contrast to the CrI spectrum, only the last spectrum shows clear splitting. We will return to this point later on. The CIII lines show different degrees of splitting, similar to the CrI lines as discussed above. The spectrum was recorded with 200 msec integration time and using 1:1 magnification (normally 1:2) with a consequent increase in the reciprocal dispersion and spectral coverage. A compromise resolving power (~0.8Å FWHM) was used for the 1:1 magnification arrangement.

Splitting of impurity lines, in particular CII and CrI, have also been observed in the early formation phase of JET discharges using a relatively short scan integration time (16.5 msec). The importance of these results will be discussed below.

It is, perhaps, noteworthy that no deliberate effort was made to enhance the Zeeman splitting effects by the use of polarising filters or by operating the spectrometer system at its maximum achieved resolution (0.7Å FWHM resolution was commonly used to obtain good S/N ratios, over a wide spectral range (3900Å-7000Å), instead of an achieved 0.3Å FWHM which would be more appropriate for observing Doppler and Zeeman effects). Thus, the results presented here should be seen quite easily in other tokamaks using similar apparatus and light collection optics.

4. ZEEMAN SPLITTING CALCULATIONS

4.1 Preamble

An atom, or ion, placed in a magnetic field suffers a splitting of its energy levels. The quantum rules governing the magnitude of the splitting, the resulting line intensities and polarisation properties of the emitted Zeeman splitted lines are discussed in some detail in standard texts (e.g. Shore and Menzel (1968) and Pauling and Goudsmit (1930)). Here we recall sufficient of the theory to interpret our observations.

The shifts in energy of the new states, from the original degenerate ones, depend on the magnetic quantum number, m, the Lande g factor and the magnetic field intensity. When the splitting is the same for the upper and lower energy levels of a transition then the 'normal' Zeeman spectral pattern of three spectral lines is observed, viz. a central unshifted line (π components) and equally shifted lines on each side (σ components). The transitions corresponding to the former suffer no change of magnetic quantum number, ($\Delta m=0$), while the latter require changes of $\Delta m = \pm 1$. The polarisation of the lines also differ. The π components are plane polarised parallel to the magnetic field and, therefore, are not observed along the field direction. The σ components vary from being plane polarised perpendicular to the field direction when viewed at right angles to the field and circularly polarised when viewed parallel to the field.

However, the π and σ components will generally consist of separate lines from several transitions involving a range of m values and, when the splitting of the upper and lower quantum states are different, several distinct π and σ lines will be emitted ('anomalous' Zeeman pattern). In fact, the designation of 'anomalous' is historical since this is the more usual case of Zeeman splitting.

An example of Zeeman splitting of the upper and lower energy levels is schematically shown in Fig.8 for the CrI ($^7S_3$-$^7P^0_2$) transition at 4289Å. In this case the increment in Mg separating the sub levels in the lower level is 2 while that of the upper level is 7/3. This difference in the energy level splitting gives a unique wavelength to each of the detailed transitions. The relative intensities of the π and σ components are represented by the heights of the vertical lines.

The relative intensities of the π and σ components, as a function of the inclination angle, Θ, the field direction makes with the viewing chord, is the same for all the transitions examined below, (i.e. dipole transitions), and are given by (e.g. Shore and Menzel (1968)):-

$$I_\pi(\Theta) \propto \mathrm{Sin}^2\Theta$$

$$I_{\sigma}(\Theta) \propto (1 + \mathrm{Cos}^2\Theta)$$

The splitting of the energy levels and the intensities of the individual Zeeman components depend on the particular electron configurations that obtain in the upper and lower states. To illustrate the main features involved, however, it is sufficient here to consider only one case in detail. We choose the CrI resonant multiplet since this shows the most convincing evidence for Zeeman splitting on JET.

The change in energy, ΔW_M, of a state with a total magnetic quantum number M ('m' is used to represent a single electron configuration) in the presence of a magnetic field B is given by:-

$$\Delta W_M = M.g.\mu_B B$$

where $\mu_B = 9.27 \times 10^{-24}\ [JT^{-1}] \equiv$ Bohr Magneton

In the presence of a magnetic field, B, the change in energy, dE, in a transition is obtained from:-

$$dE = \Delta(Mg)\ \mu_B B$$

where $\Delta(Mg)$ is the difference in the product of M and g between the lower and upper states of a transition. In wavelength terms we have, numerically:-

$$d\lambda = 4.67 \times 10^{-9}\ \Delta(Mg)\ B\lambda^2\ (\text{Å},T)$$

The magnitude of the Lande g factor depends on the electron configuration of the lower and upper states which determine the type of spin-orbit coupling that dominates (e.g. Russel - Saunders, or LS-coupling). The character of the coupling changes as the magnetic field intensity, B, increases. For large values of B, the change in energy of the atom, or ion, in the magnetic field can become much greater than the spin-orbit interaction energy. In such circumstances, at least some of the Zeeman components from the individual transitions in a multiplet will overlap with those from neighbouring lines. When this occurs the spin-orbit coupling can be neglected, for most calculations of interest, and the splitting (now referred to as the Paschen-Back

effect) is determined directly from the magnetic quantum number. This can be derived separately from the total orbit and spin quantum numbers. So the designation of 'strong' or 'weak' to a magnetic field is not related to some absolute value, but depends on the particular transition under consideration. For the magnetic field strengths and the transitions described in the paper, the coupling schemes and relative field strengths were: CrI, CIII and CII (6578Å and 6583Å):- LS-coupling, weak field; Hα (6563 Å):- ℓs interaction, strong field and CII 4267Å ($^2D_{3/2,5/2} - {}^2F_{5/2,7/2}$):- LS-coupling, strong field.

4.2 Zeeman Component Intensities

In the case of LS-coupling and weak magnetic fields, the intensities of the individual Zeeman components are summarized in Table I.

Table I Calculated relative intensities of Zeeman components for LS-coupling and weak magnetic fields.

TRANSITION	$M \to M$ (π components)	$M \to M \pm 1$ (σ components)
	Intensity	Intensity
$J \to J-1$	$C_{J-1}\ (J^2-M^2)\sin^2\Theta$	$C_{J-1}(J\mp M)(J\mp M-1)(1+\cos^2\Theta)/4$
$J \to J$	$C_J\ M^2\ \sin^2\Theta$	$C_J\ (J\mp M)(J\pm M+1)\ (1+\cos^2\Theta)/4$
$J \to J+1$	$C_{J+1}\{(J+1)^2-M^2)\}\sin^2\Theta$	$C_{J+1}(J\pm M+1)(J\pm M+2)(1+\cos^2\Theta)/4$

The constants C_{J-1}, C_J and C_{J+1} depend on the particular transition and are given by

$$C_{J-1} = I_{T,J-1}/[2\{(2J+1)J^2 - \sum_{-J}^{+J} K^2\}]$$

$$C_J = I_{T,J}/(2 \sum_{-J}^{+J} K^2)$$

$$C_{J+1} = I_{T,J+1}/[2\{(2J+1)(J+1)^2 - \sum_{-J}^{+J} K^2\}]$$

where $I_{T,J-1}$, $I_{T,J}$ and $I_{T,J+1}$ are the total intensities of the $J \rightarrow J-1$ $J \rightarrow J$ and $J \rightarrow J+1$ transitions, respectively, and K is a free parameter.

(Throughout, we follow the usual convention of allocating the lower energy state to the L.H.S. of the "→" symbol.)

The quantum number J is given by:-

$$J = L + S, L + S - 1, \ldots, |L-S|$$

where L ≡ total orbit quantum number

and S ≡ total electron spin quantum number

The magnetic quantum number, M, assumes a range of values for each J given by:-

$$M = J, J-1, \ldots, -J$$

As it happens, the CrI transitions observed in JET involve all three transitions listed in Table I.The transitions are:- $S_3 \rightarrow P_{2,3,4}$

or (L=0; J=3) → (L=1; J=2,3,4)

with λ_2 = 4289Å - $^7P_2^\circ$

λ_3 = 4274Å - $^7P_3^\circ$

λ_4 = 4254Å - $^7P_4^\circ$

The total intensities of the individual lines (e.g. the three lines from CrI multiplet) for LS-coupling are obtained from Table II.

Table II Calculated relative intensities of n, L → n′, L and n,L → n′ L + 1 transitions for LS-coupling.

TRANSITION	INTENSITY
L→L	
J → J - 1	$-\frac{(L+J+S+1)\,(L+J-S)\,(L-J+S+1)\,(L-J-S)}{J}$
J → J	$\frac{[L(L+1)+J(J+1)-S(S+1)]^2(2J+1)}{J(J+1)}$
J → J+1	$\frac{-(L+J+S+2)\,(L+J-S+1)\,(L-J+S)(L-J-S-1))}{J+1}$
L → L+1	
J → J-1	$\frac{(L-J+S+2)\,(L-J+S+1)(L-J-S+1)(L-J-S)}{J}$
J → J	$\frac{-(L+J+S+2)(L+J-S+1)(L-J+S+1)(L-J-S)\,(2J+1)}{J(J+1)}$
J → J+1	$\frac{(L+J+S+3)(L+J+S+2)(L+J-S+2)(L+J-S+1)}{J+1}$

The relative intensities of the observed spectral lines can be

calculated from Table II and yield in the case of the CrI lines:-

$$I_{T,2}: I_{T,3}: I_{T,4} :: 10: 14: 18$$

(These are more commonly known as the relative 'oscillator strengths' and they correspond to those measured experimentally and available in standard tables.)

We calculate from Table I:-

$$C_2: C_3: C_4 :: 4: 7: 3.$$

We can now give the relative intensities of the individual Zeeman components of the CrI multiplet.

Each component involves a single transition with the corresponding relative intensities (at $\theta=90^{o}$ cf. Table I):-

I_2 = (72), (64), (40), 60, 40, 24, 12, 4 ...CrI 4289Å

I_3 = (14), (56), (126), 21, 35, 42, 42, 35, 21 ...CrI 4274Å

I_4 = (96), (90), (72), (42), 84, 63, 45, 30, 18, 9, 3 ..CrI 4254Å

where the bracketed quantities refer to the π components.

4.3 Zeeman Component Line Shifts

For LS-coupling and weak magnetic fields the Lande g factor is given by

$$g = 1 + \frac{J(J+1) + S(S+1) - L(L+1)}{2J(J+1)}$$

The g factors for the CrI states $^7S_3$, $^7P_2$, $^7P_3$, and $^7P_4$ are 2, $\frac{7}{3}$, $\frac{23}{12}$ and $\frac{7}{4}$ respectively.

So applying the general selection rules $\Delta M = 0$ (π components) and $\Delta M = \pm 1$ (σ components) we obtain the $\Delta(Mg)$'s corresponding to the various Zeeman components from which the wavelength shifts are obtained. These are:-

$$\Delta(Mg)_2 = \pm \frac{(0),\ (1),\ (2),\ 4,\ 5,\ 6,\ 7,\ 8}{3} \qquad \text{..CrI 4289Å}$$

$$\Delta(Mg)_3 = \pm \frac{(1),\ (2),\ (3),\ 21,\ 22,\ 23,\ 24,\ 25,\ 26}{12} \qquad \text{..CrI 4274Å}$$

$$\Delta(Mg)_4 = \pm \frac{(0),\ (1),\ (2),\ (3),\ 4,\ 5,\ 6,\ 7,\ 8,\ 9,\ 10}{4} \qquad \text{..CrI 4254Å}$$

where the bracketed quantities refer to the π components. (The $\pm$ signifies energy shifts on both sides of the transition energy at zero field. The intensities calculated are for each component and for $\Delta(Mg)=0$ there is, of course, but one component.) The other relevant lines have the following coefficients:-

$$\Delta(Mg)_1 = \pm\frac{(0),\ (1),\ 3,\ 4,\ 5}{2} \qquad \text{..CIII 4819Å}$$

$$I_1 = (24),\ (18),\ 18,\ 9,\ 3$$

$$\Delta(Mg)_2 = \pm\frac{(1),\ (2),\ 10,\ 11,\ 12,\ 13}{6} \qquad \text{..CIII 4810Å}$$

$$I_2 = (10),\ (40),\ 10,\ 15,\ 15,\ 10$$

$$\Delta(Mg_3) = \pm\frac{(0),\ (1),\ (2),\ 3,\ 4,\ 5,\ 6,\ 7}{3} \qquad \text{..CIII 4795Å}$$

$$I_3 = (36),\ (32),\ (20),\ 30,\ 20,\ 12,\ 6,\ 2$$

$$I_{\frac{1}{2}} = (2),\ 2$$

$$\Delta(Mg)_{\frac{1}{2}} = \pm \frac{(2),\ 4}{3} \qquad \text{... CII 6582Å}$$

$$I_{3/2} = (4),\ 3,\ 1$$

$$\Delta(Mg)_{3/2} = \pm \frac{(1),\ 3,\ 5}{3} \qquad \text{... CII 6578Å}$$

I = (2), 1

...Hα 6563Å, CII 4267Å

Δ(Mg) = ± (0), 1

5. NUMERICAL SIMULATION OF ZEEMAN SPLITTING

The distributions of the toroidal and poloidal magnetic fields are represented in Fig.9 for typical operating conditions in tokamak and Reversed Field Pinch devices. The most important factors which determine the distributions are the ratio of plasma current to toroidal field flux, the ratio of kinetic to magnetic pressure (β), the plasma equilibrium position and the plasma shape. In the case of tokamaks, it is mainly the poloidal field which is sensitive to the operating conditions and since it is <10% of the toroidal field, approximate values suffice when calculating the total magnetic field vectors. It is also sufficiently accurate for our purposes here, to neglect the slight plasma para- or dia-magnetism when calculating the toroidal magnetic field since the poloidal current in the plasma warrants at most, a 10% correction to the vacuum field. The corrections are much smaller at the plasma periphery which is of most relevance in this paper.

Reversed Field Pinches exhibit more complex field configurations where the plasma plays a comparable role to the external circuits in determining the toroidal and poloidal field distributions. However, in present machines at least, the total field intensities are an order of magnitude lower than in tokamaks so that Zeeman splitting effects are generally masked by instrumental and Doppler broadening effects. Again, the plasma periphery is the more important region in the present analysis, where the fields are determined by the total currents in the plasma and in the toroidal field coils.

For both the Reversed Field Pinch and tokamak configurations we can observe from Figs.2 and 9, that the magnetic field intensity, and its inclination angle with the viewing direction, will vary

considerably as the point of reference is moved out in radius from the machine centre-line. An illustrative example, from JET, of the field intensity and its inclination angle, at various radial positions is shown in Fig.10. The tangential viewing optics described in Fig.2 is assumed and the relatively weak poloidal field ($B_{pol}/B_{tor} \lesssim 0.1$) is ignored in these calculations.

The results of the calculations are displayed in Fig.11 for various transitions of interest. In accordance with convention, the intensities of the π and σ components are represented by the heights of the vertical lines whose spectral positions are determined by the Zeeman shifts. (For the sake of clarity, the central π components are represented by 'negative' intensities.) These calculations refer to the 'tangential' viewing optics arrangement on JET where the tangential radius, of the line of sight to the machine centre-line, was at 2.12 m. The toroidal field-radial position product was 6.39 tesla-metres. The Zeeman pattern from an element of plasma is examined at incremental steps of 0.5m in the major radius, starting at 2.12 m. At this position the magnetic field is almost parallel to the viewing direction. The same distributions of field and inclination angles, as shown in Fig.10, are used in these calculations. As expected, at the radii close to the tangential radius the σ components dominate and as the major radius increases the splitting decreases as does the relative intensity of the σ components when compared with the π components.

The total line profiles can now be calculated from the measured instrumental function, the magnetic field intensity and the inclination angle distribution. We show examples of such calculations in Fig.12 for the same set of lines and conditions as described in Fig.11. (The intensity of the CII line at 6583Å is doubled in the computations and the relative intensities between the sets of lines corresponding to the different elements are chosen to maintain overall clarity.) Each Zeeman component has a spectral profile given by the measured instrumental function. The total line profile is obtained by summing all the components, irrespective of their polarisation. This is appropriate because of the depolarising effects of the fibre optic link (cf.Section 2 above).

We note that the relative intensities of the lines, which were calculated by using an LS-coupling model and assuming statistical population of all the levels and sub-levels, in the CrI, CIII and CII multiplets in Fig.12 are in good agreements with those found experimentally. Individual Zeeman components should not be directly observed apart from the CII line at 6583Å and $H\alpha$ at 6563Å, under present circumstances.

The overall splitting of the lines should,therefore,not be directly observed for the CrI lines where $R \gtrsim 2.6$m with the present arrangements and field strengths. In JET it is found that the carbon limiters are generally the dominant sources of chromium and carbon and because of the short ionisation times of CrI → CrII and CII → CIII (typically 2μs and 700μs respectively, with corresponding ionisation lengths of 1cm and 60cm) these plasma regions will be the brightest at the CrI and CII lines for a machine with the dimensions of JET. Thus, in general, the detected spectral lines will not exhibit Zeeman splitting in JET with the exception of the CII 6583Å line which should show some structure for typical field intensities (cf. Fig.4) at the outer plasma periphery where the limiters are located.

However, there will be occasions when the plasma inner periphery will be relatively bright, for example, when the plasma interacts with the inner wall, or when large particle fluxes (e.g. neutral atoms) impinge on the walls remote from the plasma, with a consequent release of wall materials and accumulated hydrogen. The inner plasma periphery may then be the brightest at the CII and CrI lines and this should facilitate the observation of Zeeman splitting. The subsequent movement of this inner plasma periphery may be monitored with the simple model described, until the contribution to the relevant lines from the carbon limiters becomes comparable. In this case, a composite spectrum should be calculated to include the contributions from all the plasma edges in the line of sight.

Improvements in the optics-spectrometer arrangement may be easily realised which would enhance the Zeeman splitting. These may be achieved by, for example, reducing the instrumental width and employing an appropriate polarisation filter to eliminate the π components. In

the absence of the π components, the modulation of the individual spectral lines depends on the ratio of the instrumental width to the magnetic field strength. Therefore, a Zeeman pattern similar to that observed at the tangential radius (cf. Fig.12) would be detected at the limiter if the instrumental width were halved to $\sim$ 0.35Å.

6. INTERPRETATION OF RESULTS

A straightforward method of analysing the spectra which exhibit Zeeman splitting is to measure the wavelength separation of the groups of σ components either side of line centre. If it can be assumed that the π components have a negligible influence on the separation of the spectral double peaks (due to the convolving effect of the instrumental function), the magnetic field intensity can be calculated from an intensity weighted ΔMg value. Since the total magnetic field distribution in a tokamak is known (within a few %) the position of a plasma element which would give the same splitting can be calculated. The results of such an analysis are shown in Table III for a collection JET shots.

The line centres of the principle transitions are obtained from times in the JET discharge when the limiter region (where Zeeman splitting is least) dominates the emission. This allows for an accurate spectral dispersion calibration and, because the OMA and spectrometer are stationary throughout the discharge,absolute wavelength shifts can be measured. The spectral shifts of the peaks of a line, which exhibits splitting, is seen to be symmetric about the earlier line centres. The $\Delta\lambda$ used in Table III is that derived from half the peak separation. From the spectral shifts, the magnitude of the field, B, is obtained using an intensity weighted Δ(Mg) value that is derived from the Zeeman components contained within each peak. The position, R, of an emitting element at the calculated B value is determined from the known field distribution. The angle of inclination, θ, that $\vec{B}$ makes with the viewing direction is obtained from simple geometrical calculations (cf. Fig.10). In this analysis the ratio of the total intensities from the π and σ components, $\Sigma I\pi/\Sigma I\sigma$, is calculated from θ (i.e.$\sin^2\theta/(1+\cos^2\theta)$). This ratio varies

from zero to approximately one half at the tangential radius and outer limiter positions, respectively.

It is invaluable to deconvolve the observed spectra with the measured instrumental function (obtained from a spectral lamp or a He-Ne laser source) so as to increase the effective resolving power of the spectrometer. The improvement in effective resolving power ultimately depends on the individual channel, or pixel, bandwidth (~0.1Å) compared with the overall instrumental width. The improvement in resolution that follows is particularly important when the line splitting is of the same order as the instrumental line width. We show an example of an observed and deconvolved (Carolan et al (1985)) spectrum in Fig.13 of a CrI multiplet and a CII line. We note that there is almost 100% modulation in the CrI 4274Å line which showed the greatest splitting in the directly observed spectrum but the deconvolution of the apparently featureless CrI 4254Å line also exhibits splitting from the Zeeman effect. The splitting of the three CrI lines yields the same field strength of 3.0±.1T. This is the field at 2.12 m, almost exactly coincident with the tangential radius of the viewing chord. Hence, the toroidal field is close to parallel to the viewing direction which explains the almost complete absence of the central π components (cf. especially the CrI 4274Å line). The lack of splitting in the deconvolved CII line at 4267Å could be due to the influx being predominantly at the outer periphery (where the field is weakest) at the carbon limiter or, more likely, because the light CII ions have greater Doppler broadening of their spectral lines which smears out the Zeeman splitting.

We can compare the estimates of the plasma periphery position given by that from the Zeeman splitting of the spectral lines give with that obtained from electrical measurements. Examples of computed flux surfaces (Brusati et al (1984)) of the JET plasma (Shot 831) obtained from electrical measurements, made external to the plasma, are shown in Fig.14 together with the circle of view of the spectrometer collection optics. Relatively rapid plasma movement is observed electrically which is in accord with Zeeman splitting. Good agreement is seen between the measurements which confirms that the Zeeman splitting

techniques can localise the impurities (or hydrogen) independently of other measurements.

More recently, the observation of splitting on CIII (cf. Fig.7) which located it on the inner periphery (R=2.26 m) is of particular relevance to JET. These results showed that the vacuum vessel was contaminated and not just the limiter where CIII is normally seen. We mentioned earlier that the behaviour of CIII shown in Fig.7 contrasts with that of CrI shown in Fig.6 where the large increase in line intensity was accompanied by Zeeman splitting. The middle scan of Fig. 7 shows no such splitting. We note that the relative increase in the CrI multiplet intensity (Scan 29) is very large indeed compared with the previous scan, so that the inner periphery can dominate the observed spectrum. Now the CIII spectra show line intensities, during Shot 2535, which are typically ~20% of those shown in Scan 49 in Fig.7 and this may be important in determining the detailed line shape which is composed of contributions from the outer edge and the inner periphery, provided this is within the line of sight. Actually, we use the terms "edge" and "periphery" quite loosely, but from a spectroscopic sense they refer to the plasma regions where the particular line in question peaks in emissivity. Thus, neutrals will tend to yield plasmas of larger diameter, than those from ions, and more detailed comparisons with electrical measurements are possible. The latter measurements can define the outermost magnetic surface (i.e. the first comes in contact with vessel material, e.g. an outer limiter). Nevertheless, it is at least instructive to compare the spectroscopic observations of CIII in Fig.7 with plasma inner and outer magnetic limits obtained from electrical diagnostics. These are shown in Fig.15 for the termination phase of Shot 2535. The time on the X-axis is from current initiation. The top trace shows the position of inner periphery of the plasma limiting magnetic surface, from an inner wall protection plate at R=1.705 m. The middle trace shows the position of the outer periphery with respect to an outer limiter at R=4.11 m. The decay of the plasma current Ip, during termination, is shown in the bottom trace. (The plasma current during the sustainment phase was 2.09 MA). We also show in Fig.15 the time slices corresponding to the spectral scans of Fig.7. (Checks of the

synchronisation of the JET data acquisition system and the SADA-OMA system used for our spectroscopic observations which was quite autonomous, apart from a trigger pulse, were obtained from detailed comparisons from hydrogen Balmer lines observed from the same fibre but recorded on the JET and SADA-OMA systems simultaneously.)

The initial decay of plasma current is seen in Fig.15 to be accompanied by a gentle plasma contraction where the inner periphery progressively departs from the inner wall while the outer periphery is defined by the outer limiter. Spectral Scan No. 48 is typical of this period. But scan No. 49 encompasses a more dynamic period where there is plasma expansion and contraction. This period is actually a precursor to the final disruption captured in Scan No. 50 where the plasma detaches itself from the outer limiter (cf. middle trace) and the inner wall protection plate defines the new limiting magnetic surface. The general disruptive nature of this period is most clearly seen in the rapid current decay. From the spectroscopic point of view, the plasma detachment from the outer limiter is significant since the injection of chlorine from this source should be correspondingly reduced which aids the observation of Zeeman splitting as seen in Scan No. 50. However, we should also note that in this period the inner position of the limiting magnetic surface (R=1.71 m) is well to the inside of the tangential radius position at R=2.12 m or the estimated position of ClII at R~2.26 m. There can be various reasons why the presence of ClII so far from the plasma periphery during the plasma disruption and final decay. For example, the impurity cross field transport may be enhanced so that ClII is far from being in coronal equilibrium with the background electron temperature or the latter is reduced during and following a disruption.

It is probably of little profit to examine this aspect in more detail due to the lack of data (e.g. because of the course 200 msec spectral time slices) and the difficulty of analysing transient disruptive phenomena. The splitting observed in Scan 50 of Fig.7, which is absent in Scan 49, highlights the role played by both the inner and outer plasma peripheries in determining the final line structure. So if the outer periphery were separately monitored it should be possible to subtract

its effect from the composite spectrum and so observe the behaviour of the inner periphery. Unfortunately, this facility was not available. Nevertheless, The main conclusion we wish to draw from the ClII behaviour therefore seems secure, viz. the plasma vessel was contaminated with chlorine and not just the outer limiter for this later series of JET shots.

The localisation of CrI and CII on the inner plasma periphery during the early setting up phase of the discharge (cf. Table III for shots 2403 and 2453) emphasises the role of the vacuum vessel wall in producing impurities. The particular observation of splitting on CII, which localised it at R=3.51 m, shows that this technique may be used to monitor the inner plasma periphery of small cross section plasmas (e.g. during setting-up). This can be particularly important during plasma formation when, because of the relatively small plasma currents and cross sections, electrical diagnostics may not be sufficient to accurately locate the plasma edges.

7. SUMMARY OF RESULTS

The main points to note from the Zeeman splitting of the spectral lines are that

(a) different transitions from the same element yield very similar values of B;

(b) changes of the plasma position, at least of that region which dominates the emission, are observed from the different spectral scans;

(c) different ions, or neutrals, are not necessarily located at the same plasma position (cf. HI and CII) following a major plasma excursion or from particle influxes from the vessel wall which can be remote from the plasma edge;

(d) although the splitting observed in the CrI lines shows that CrI is located at the inner plasma periphery, the plasma is not in contact with the inner wall otherwise the short ionisation length of CrI to CrII (~1 cm) would prevent it from being observed with

the present optical arrangement. Neither can CrI be entirely due to earlier contact with the wall because of the short ionisation time (~2μs). Although recombination from CrII may contribute, the more plausible explanation is that the CrI is sputtered from the inner wall and travels on free trajectory paths to the plasma periphery where it is excited and ionised.

(e) influxes of impurities from either the inner or outer wall positions can be distinguished, even along a single line of sight spectrometer, by their different Zeeman splitting.

8. CONCLUSIONS

Zeeman splitting of impurity and hydrogen spectral lines has been directly observed, we believe for the first time, in a tokamak plasma. Consistent values of the toroidal field strength are observed from the separate line spectral profiles. Thus, the location of the emitting species can be determined from the known field distribution. Even when, due to instrumental or field configurations, Zeeman splitting is not immediately observed from the raw data, it may often be necessary to include its effects, especially in tokamaks, when interpreting the broadening of visible transitions.

The techniques described herein can be easily applied since only commercially available optics, spectrometers and detectors were used. Simple improvements (e.g. a polariser to eliminate the central π components) in the system will allow such observations to be made over a wide range of operating conditions.

9. ACKNOWLEDGEMENTS

The authors would like to thank their JET and Culham Laboratory colleagues especially Drs K Behringer, W Engelhardt, J Hugill and P D Morgan, who also provided the fibre optical link, for invaluable discussions and assistance. We also gratefully acknowledge the data from the magnetic diagnostics provided by Dr B de Kock and his group. The magnetic flux surface calculations were made by Drs M Brusati,

J P Christiansen and E Lazzaro from JET. The OMA control software was written by I Dewa of Teeside Polytechnic, Middlesborough. The deconvolution was performed by Drs S F Gull and A Williams of St John's College Cambridge University.

The work was carried out under a Task Agreement between JET and Culham Laboratory.

Table III Analysis of spectra which show clear Zeeman splitting. $\Delta\lambda$ is the separation of peaks from line centre and B(ZMAN) is derived from $\Delta\lambda$ using an intensity weighted Lande g factor. The influence of the central π component on the peak locations is assumed to be negligible and the emission is considered to originate from a single plasma element at R(ELMT) obtained from B(ZMAN). θ is the angle between $\vec{B}$ and the viewing direction and is obtained from the location of the emitting element and simple geometrical calculations. The ratio of intensities of the π to σ components, $\Sigma I\pi/\Sigma I\sigma$, is calculated from θ; t is the time in the discharge corresponding to the spectral mean time and B_ϕ is the toroidal field on axis (R = 2.96m).

Shot No	Scan	ELMT	λ (Å)	$\Delta\lambda$ (Å)	B (ZMAN) (T)	R (ELMT) (m)	θ (deg)	$\frac{\sum I\pi}{\sum I\sigma}$	t (sec)	B_ϕ (axis) (T)
831	29	CrI	4274	0.51	2.99	)2.11	0	0	1.33	2.16
	29	CrI	4289	0.44	3.08	)				
	30	CrI	4274	0.40	2.33	)2.72	38	0.23	1.38	
	30	CrI	4289	0.34	2.28	)				
838	26	CII	6583	0.60	2.22	)2.97	44	0.32	1.18	2.16
	26	CII	6578	0.42	2.09	)				
	27	CII	6583	0.66	2.45	)2.56	33	0.17		
	27	CII	6578	0.51	2.53	)			1.23	
	28	CII	6583	0.72	2.66	)				
	28	CII	6578	0.53	2.63	)2.46	30	0.14		
	28	HI	6563	0.44	2.17	2.96	44	0.32	1.28	
	29	HI	6563	0.35	1.74	3.72	55	0.50	1.33	
2445	19	CrI	4274	0.81	4.82	)2.12	0	0	0.03	3.39
	19	CrI	4289	0.66	4.62	)				
2453	18	CII	6583	0.58	2.15	3.51	53	0.47	0.02	2.55
2535	50	CIII	4810	0.64	3.12	)2.26	20	0.06	8.92	2.41
	50	CIII	4819	0.60	3.17	)				

References

Axon, K. B., Bradley, J. E., Burt, J., et al Plasma Physics and Controlled Nuclear Fusion Research, Vol. I, IAEA, Vienna (1983) 201 (Proc 9th Int. Conf. Baltimore USA 1982).

Breton, C., DeMichelis, C., Finkenthal, M. and Mattioli, M, J Phys B: Atom. Molec. Phys. 13 (1980) 1703-1718.

Brusati, M., Christiansen, J.P., Cordey, J.G., Jarrett, K., Lazzaro, E., and Ross, R.T., Computer Phys. Reports, 1 (1984), 345.

Carolan, P.G. et al, 10th Int. Conf on Plasma Physics and Controlled Nuclear Fusion Res., London, CN-44/D-II-3 (1984).

Carolan, P.G, Gull, S.F. and Williams, A., Paper in preparation, (1985)
'The Use of Maximum Entropy Methods in Spectroscopic Applications'

Cross, G. C., Fullard, K., Read, A. H. and Reed, K. Proc 10th Symp of Fusion Technology I (1978) 477.

Fonck, R. J, Darrow, D. S. and Jaehnig, K. P., 29 Phys. Rev. (1984) 3288

Hübner, K. Z Naturforsch 19a (1964) 111

Jahoda, F.C., Ribe, F.L. and Sawyer, G.A. Phys. Rev 131 (1963) 24

McCormick, K. et al. Proc. 8th Eur. Conf. on Controlled Fusion and Plasma Physics, 1 (1977) 140

Pauling L. and Goudsmit, S. "The Structure of Line Spectra" McGraw-Hill, N.Y.(1930).

Rebut, P.H. et al, 10th Int. Conference on Plasma Physics and Controlled Nuclear Fusion Res., London, CN-44/A-I-1 (1984)

Shore, B.W. and Menzel, D.H. "Principles of Atomic Spectra" J Wiley & Sons Inc. N.Y.(1968).

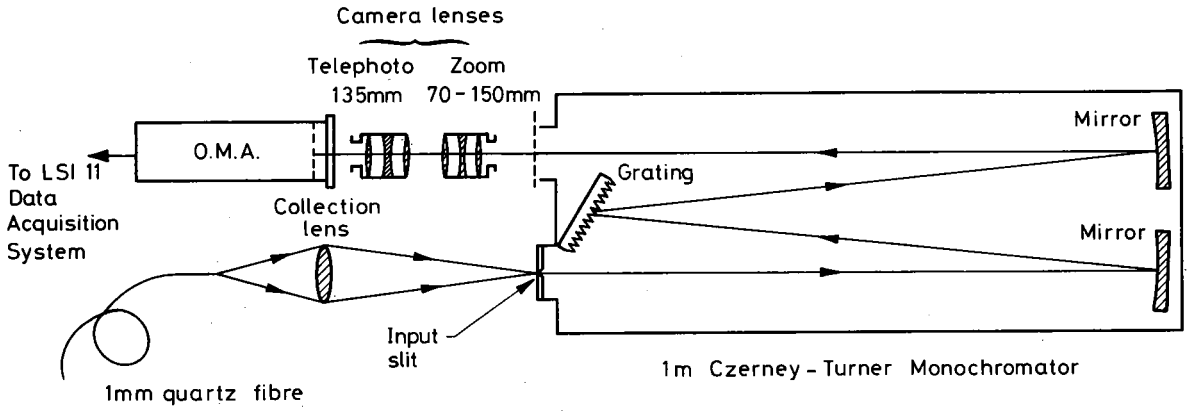

Fig. 1 Visible multichannel spectrometer. The input slit is illuminated via fibre optics from the plasma machine. Front-to-front 35 mm camera lenses control the magnification of the dispersion at the OMA.

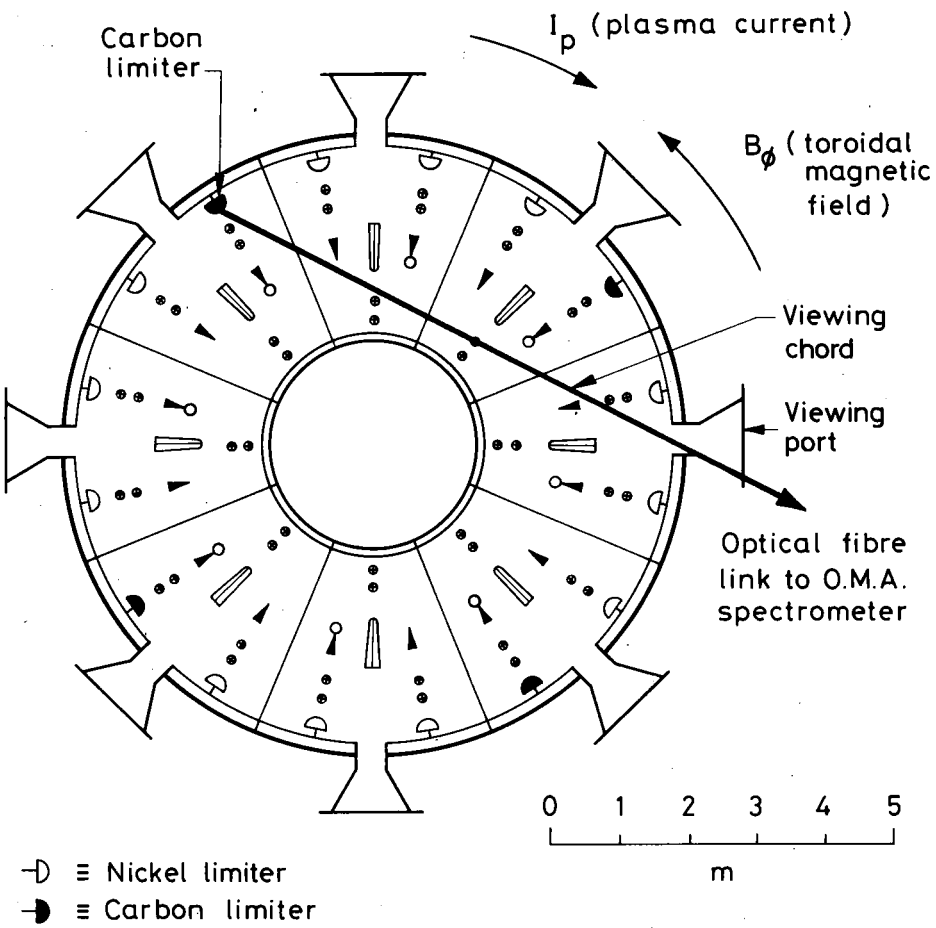

Fig. 2 A 'tangential' viewing optics arrangement in JET which obtains a clear view of the carbon limiter. This can be the dominant source of impurities in the plasma.

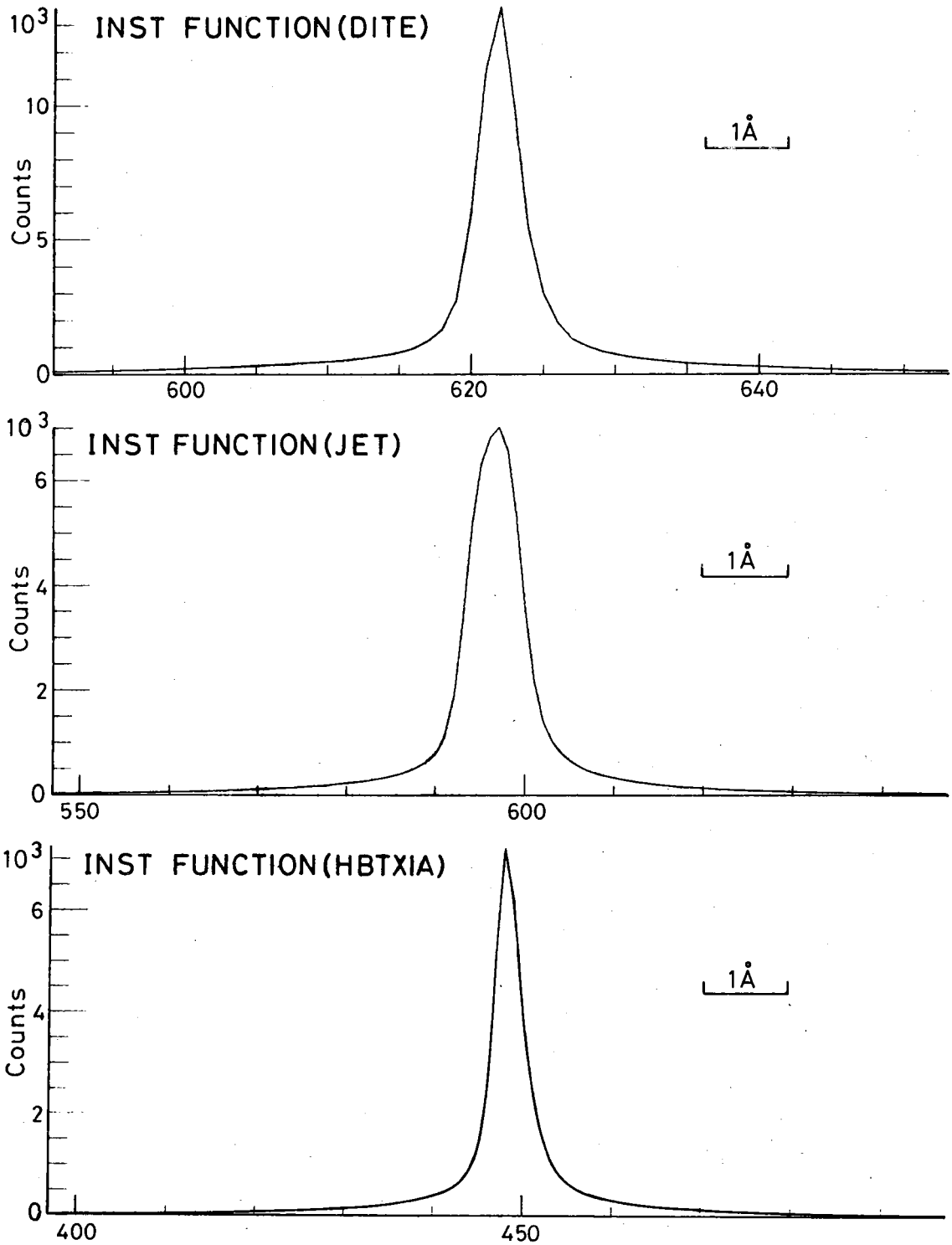

Fig.3 Typical instrumental functions of the OMA-spectrometer as used on the DITE, JET and HBTX1A machines.

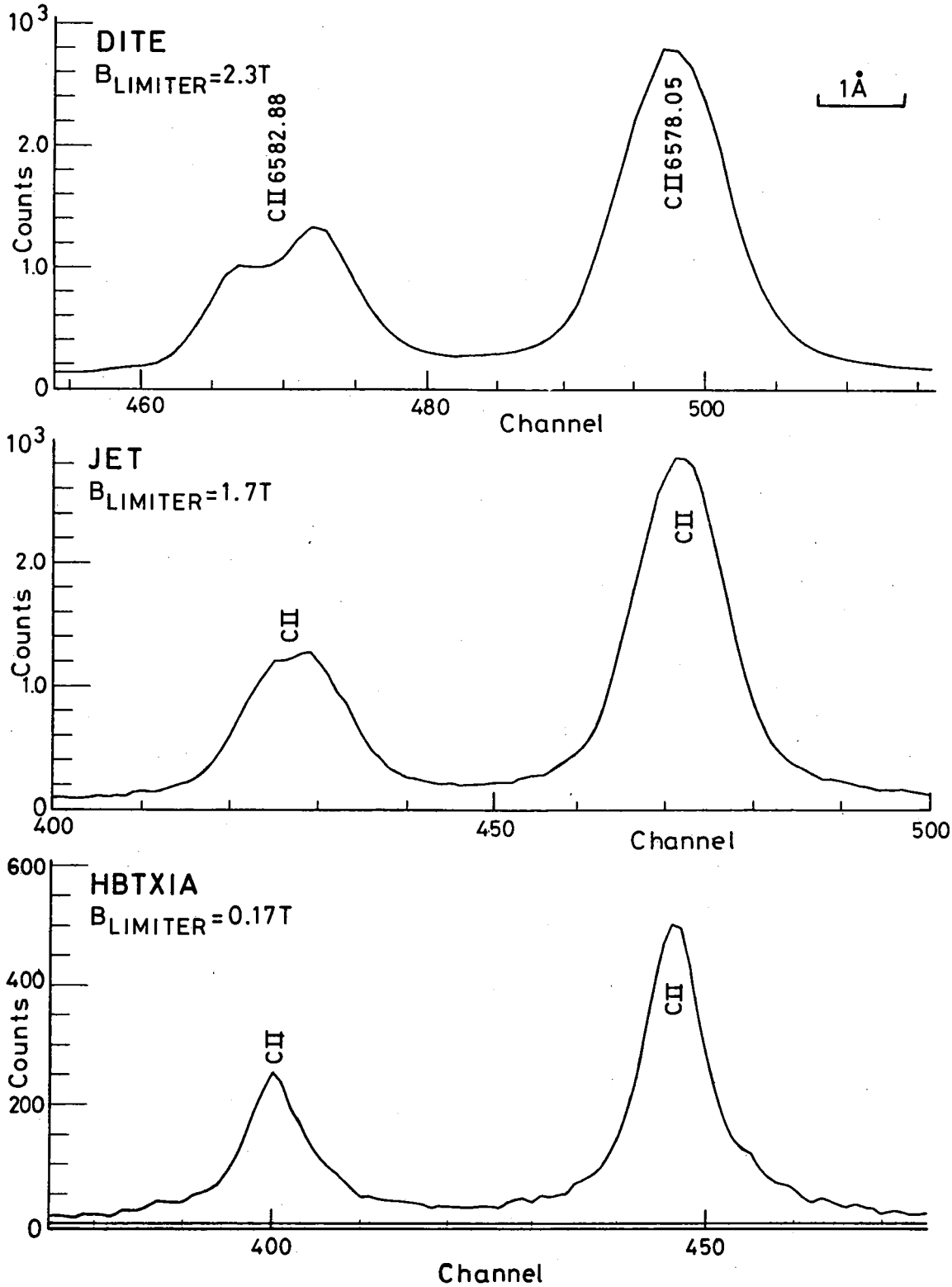

Fig.4 Detailed OMA spectra of a CII doublet ($^2S_{1/2} - {}^2P_{3/2,1/2}$) taken from the HBTX1A Reversed Field Pinch and the DITE and JET tokamak devices. The HBTX1A assembly has a total edge field of approximately 0.17T while the tokamak machines have outer edge fields of approximately 1.7T and 2.3T for JET and DITE, respectively. The Zeeman splitting expected from HBTX1A is insignificant (~ 0.05 Å).

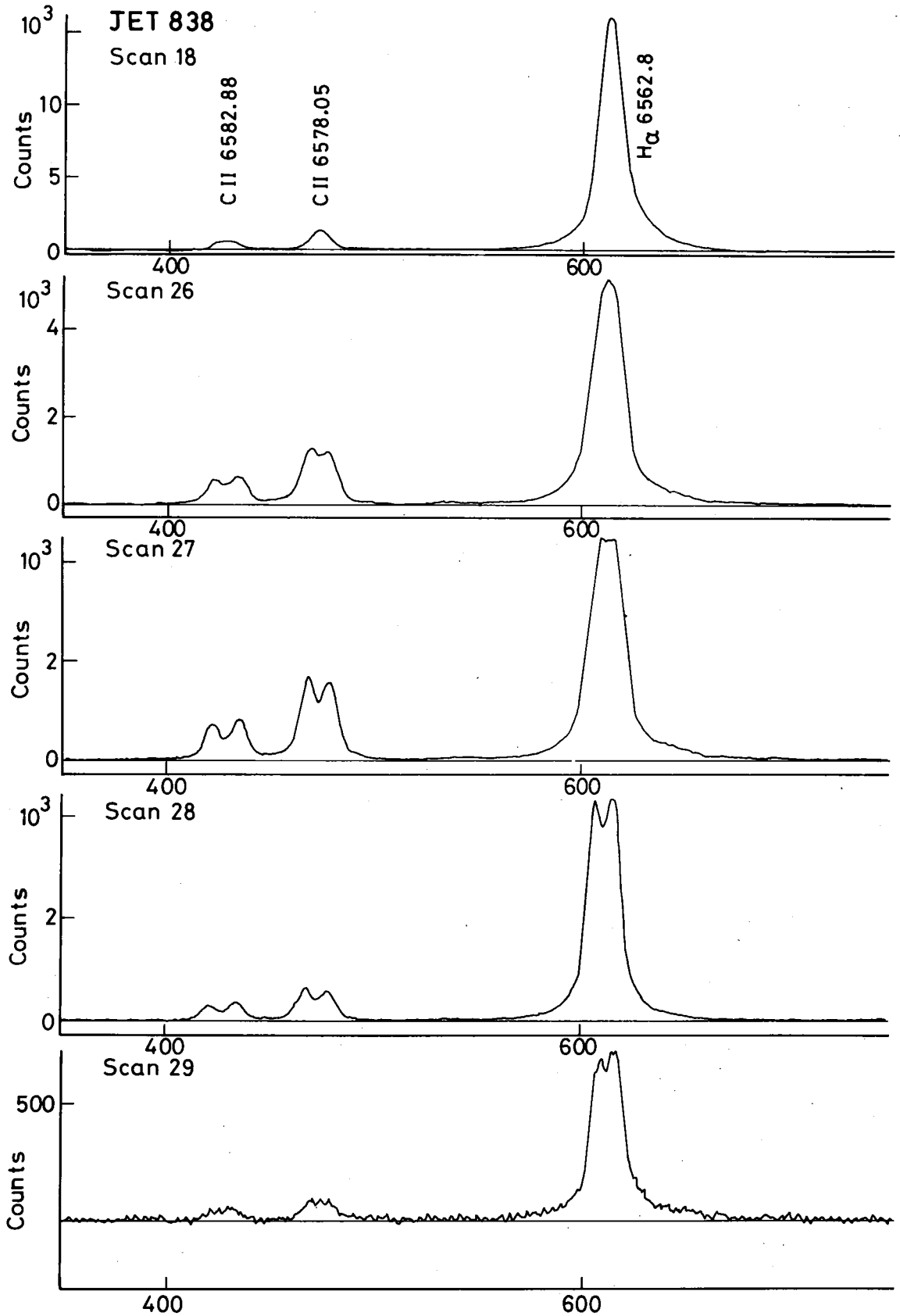

Fig.5 The first scan shown here is a reference one taken midway during the JET discharge. The remaining scans are taken at 50ms intervals, during the plasma termination phase. The spectral region encompasses the CII doublet ($^2S_{½} - {}^2P_{3/2,½}$) at 6578Å and 6583Å and the H_α (Balmer) line at 6563Å.

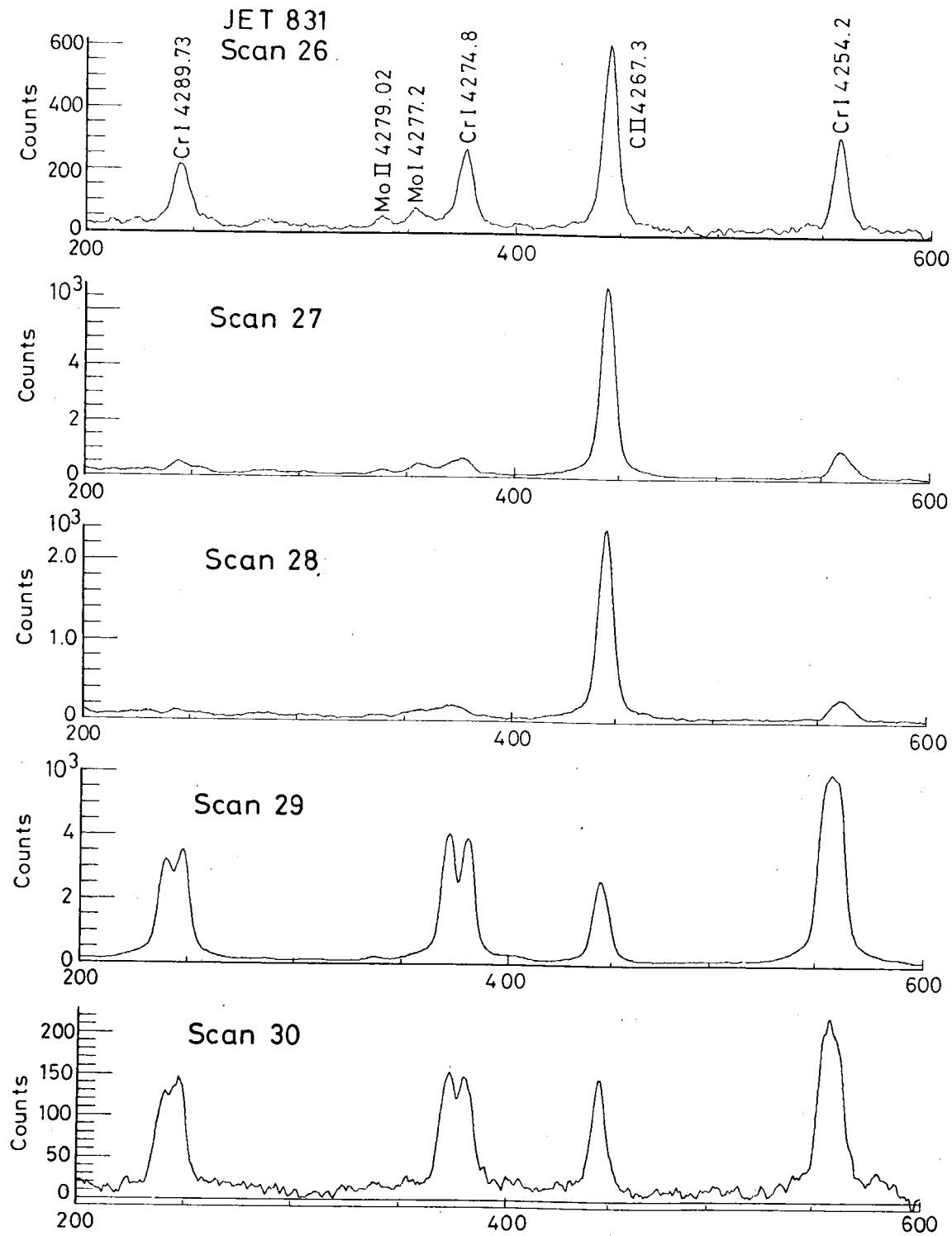

Fig.6 The spectral scans (50ms intervals) are taken from the JET experiment during the plasma termination phase. The first scan is typical of the plasma sustainment phase. The spectral region encompasses a CrI multiplet and a CII line. The various splittings observed in the CRI lines are consistent with Zeeman shifts expected for each transition for the same field strength.

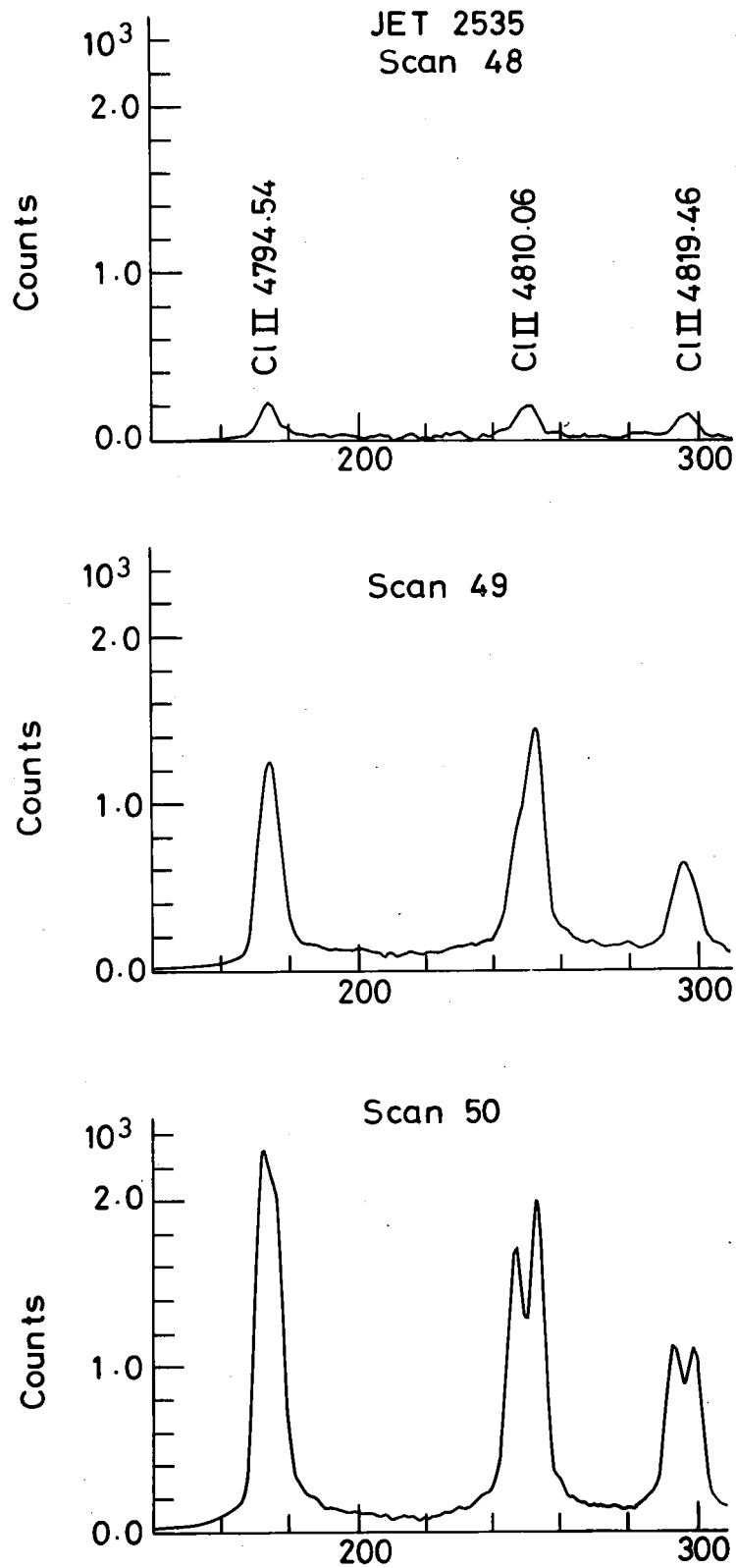

Fig.7 Three spectral scans (200ms intervals) obtained during the termination phase of a JET discharge. Similar splitting of the C1 II lines as observed from CRI can be seen. The C1 II (Scan 50) is located at 2.26m.

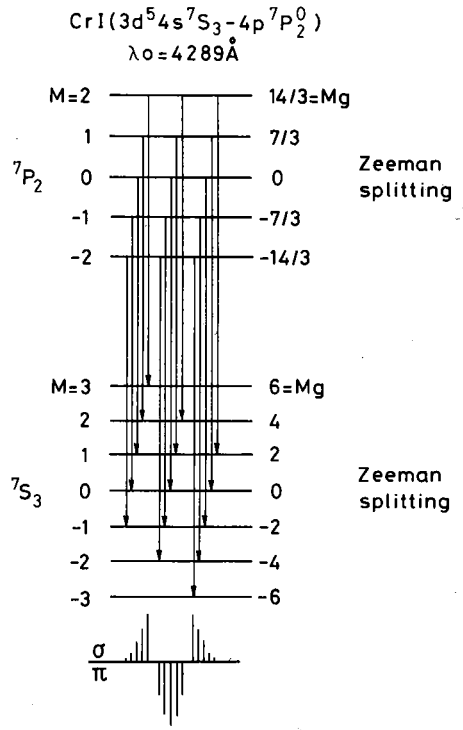

Fig.8 Schematic representation of Zeeman splitting of the lower and upper energy levels in the CRI transition at 4289 Å ($3d^5 4s^7S_3 - 4p^7P^0_2$). The $\pi(\sigma)$ component intensities shown are those obtained when the viewing direction is parallel (perpendicular) to the magnetic field direction.

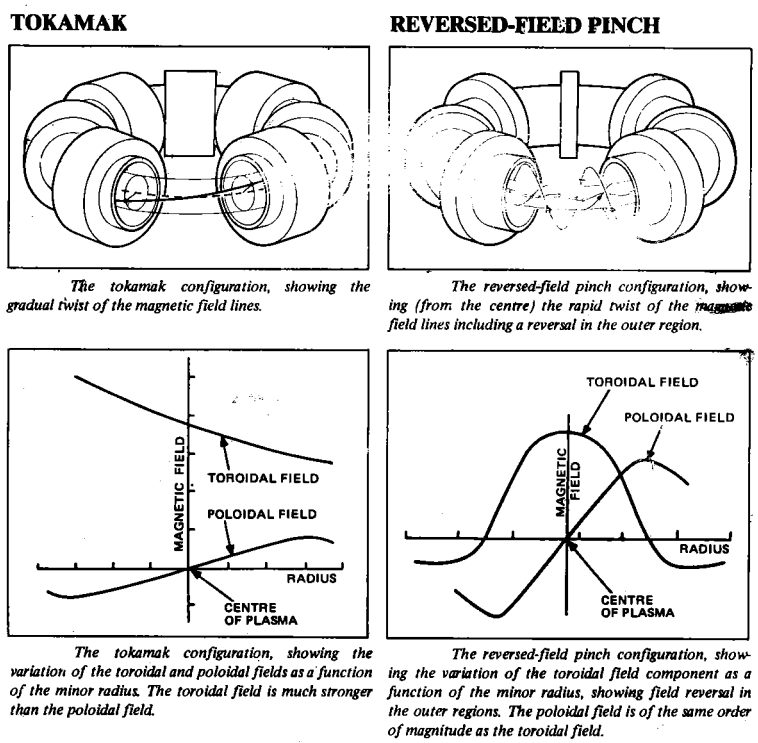

Fig.9 Toroidal and poloidal field distributions for typical operating conditions in tokamak and Reversed Field Pinch devices.

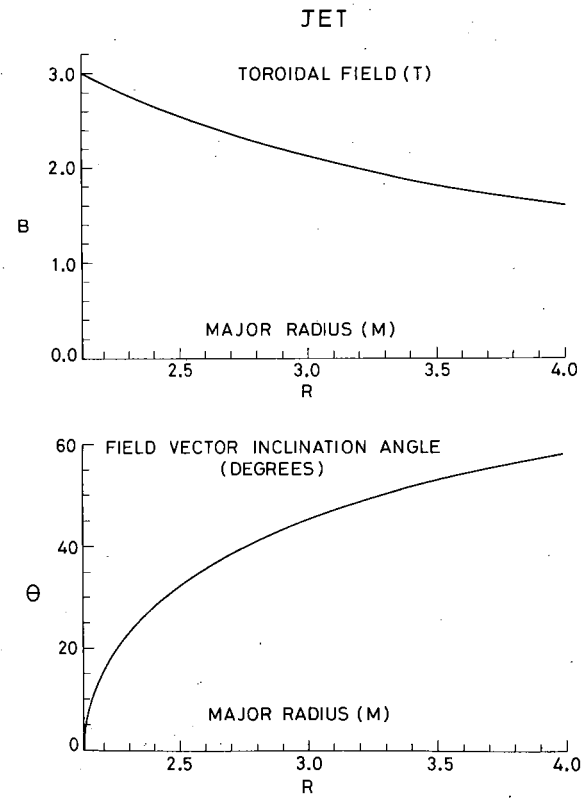

Fig. 10 Variation of the magnetic field intensity and inclination angle with the line of sight for a representative JET field configuration. The tangential radius of the tangential viewing chord was at a radius of 2.12 m.

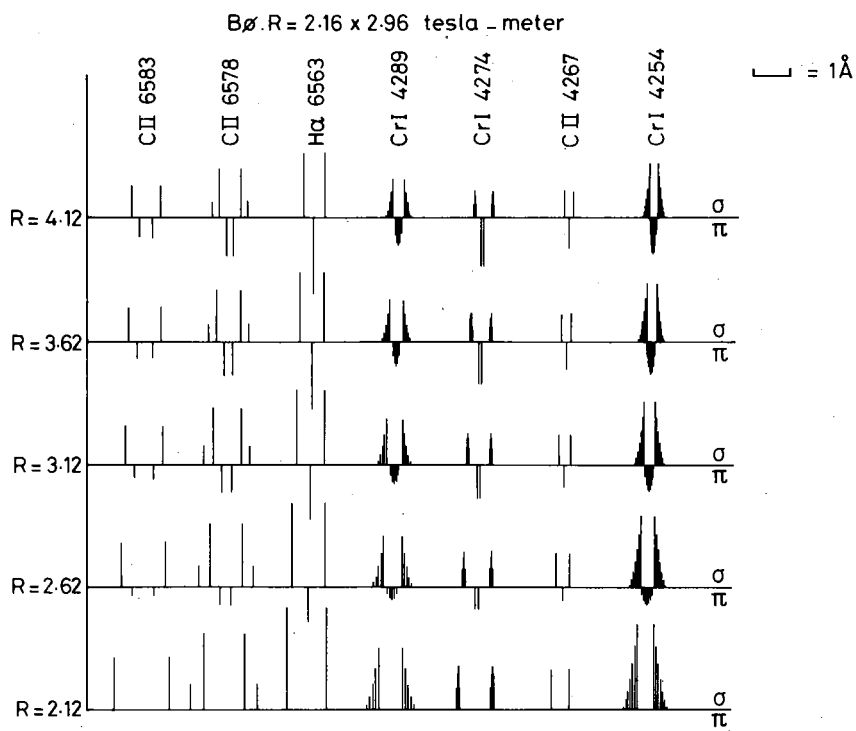

Fig. 11 Computed Zeeman patterns of selected lines at various radial positions in JET as seen by the tangential viewing optics. The lines are from the CII and CrI multiplets and H_α where Zeeman splitting has been observed. A typical field of 2.16 T is assumed at a major radius of 2.96 m. The tangential radius of the viewing chord was at a radius of 2.12 m.

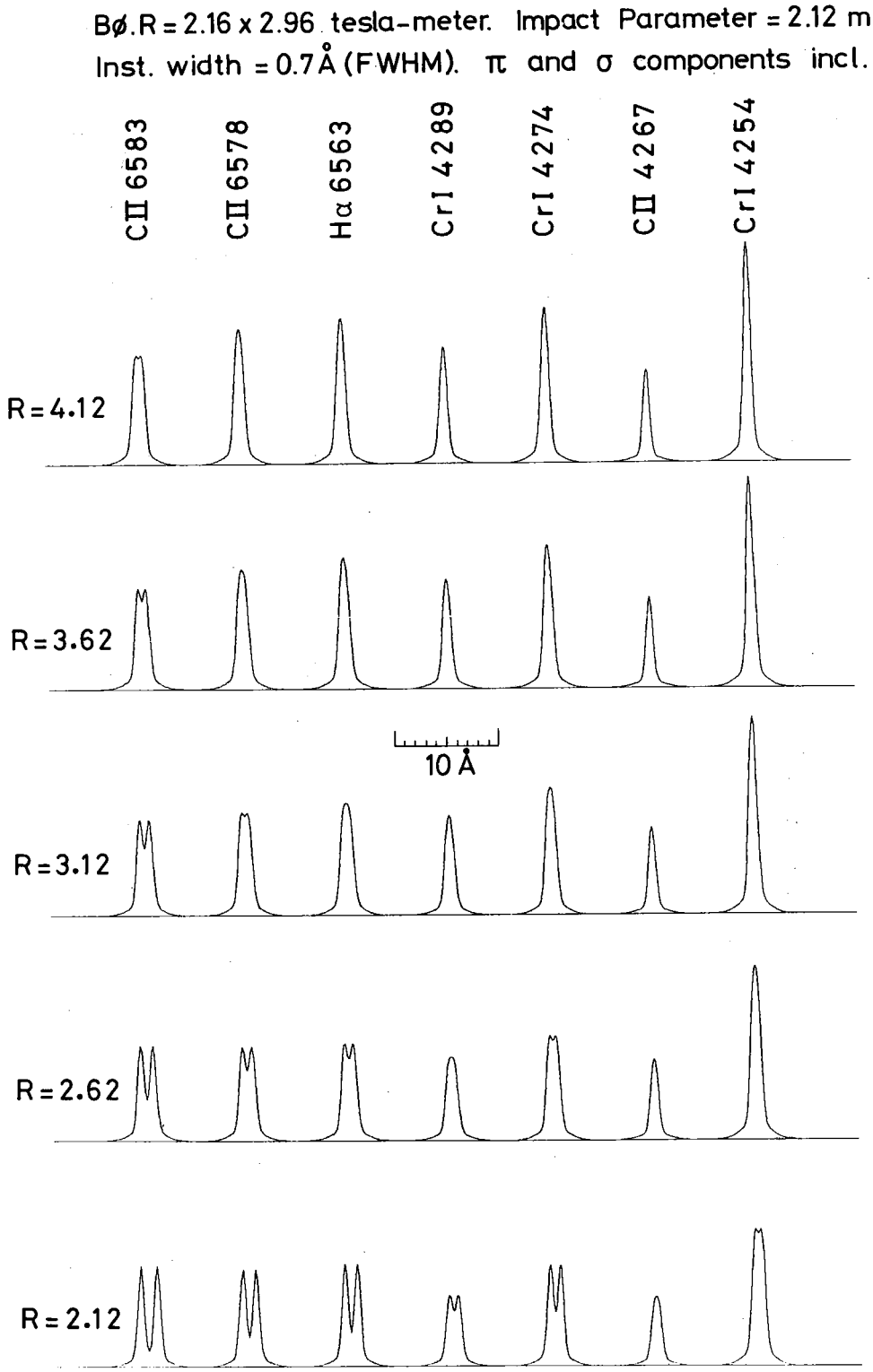

Fig. 12 Computed line profiles of the selected lines where the measured instrumental function is incorporated in the calculations. The instrument function corresponds to that used when the Zeeman splitting was observed (FWHM = 0.7 Å, cf. Fig. 3). (For clarification, the CII line intensity at 6583 Å was doubled in the computations).

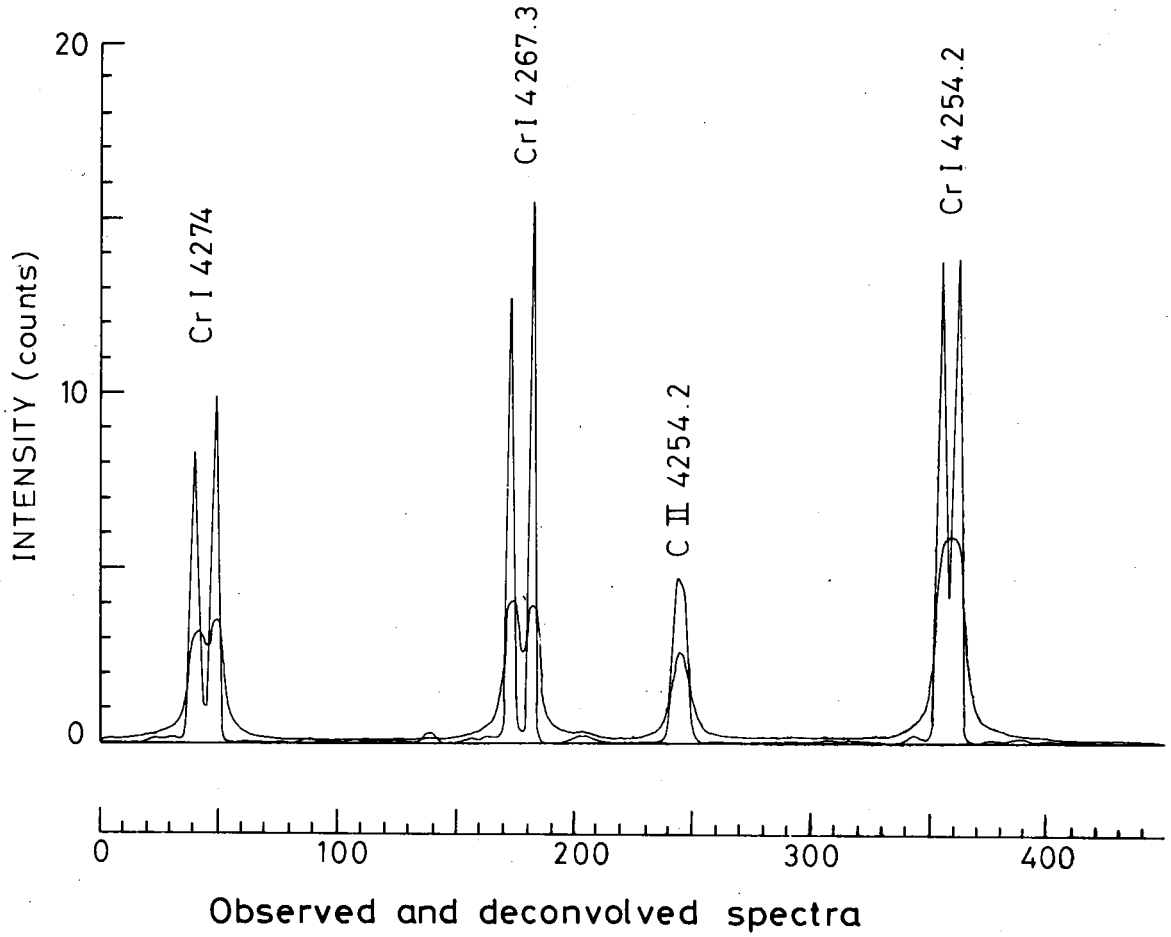

Fig. 13 Comparison between an observed spectrum which shows Zeeman splitting and a deconvolved one using the measured instrumental function and employing maximum entropy numerical techniques.

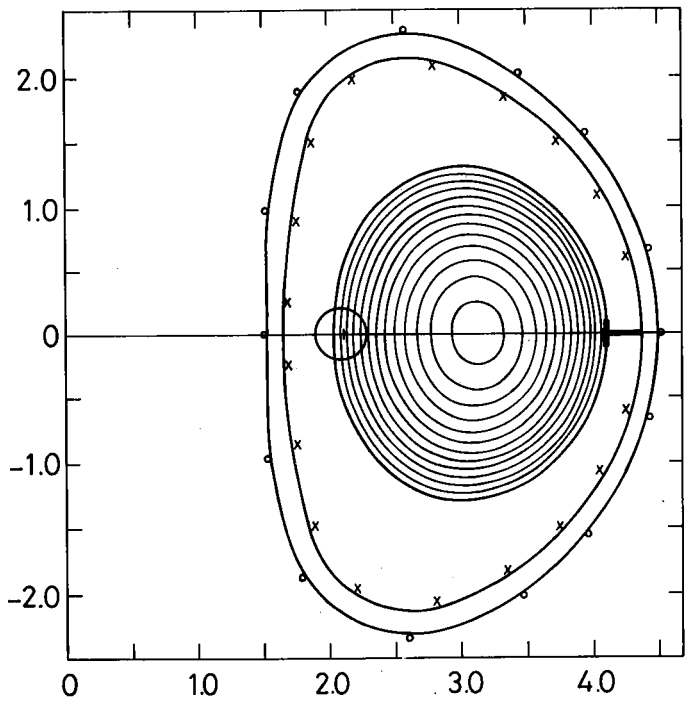

Fig. 14 Calculated magnetic surfaces of the JET plasma, during the discharge termination phase of shot 831, derived from external electrical measurements. The small circle at the periphery represents the area seen by the collection optics midway along the viewing chord.

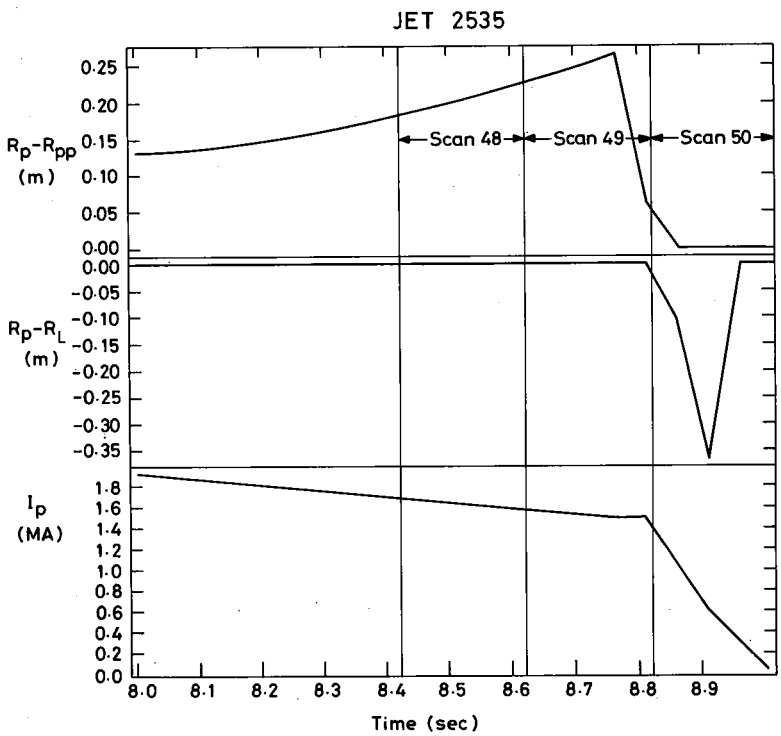

Fig. 15 Behaviour of JET shot 2535 as determined from electrical diagnostics during the termination phase. The upper and middle traces show the position of the plasma limiting magnetic surface with respect to the inner wall and the outer limiter respectively: $R_{pp}^{\equiv}$ plate protection position = 1.705 m, $R_L \equiv$ outer limiter position = 4.11 m and R_p is the inner or outer plasma periphery position, respectively; $I_p \equiv$ plasma current. The time shown is from current initiation. The time slices occupied by the spectral scans of Fig. 7 are also shown.